

# Secrecy Analysis of Physical Layer over $\kappa - \mu$ Shadowed Fading Scenarios

Hussien Al-Hmood, *Member, IEEE*, and H. S. Al-Raweshidy, *Senior Member, IEEE*

## Abstract

In this paper, the secrecy analysis of physical layer when both the main and wiretap channels undergo  $\kappa - \mu$  shadowed fading channel is investigated. In particular, the average secrecy capacity (ASC), secure outage probability (SOP), the lower bound of SOP ( $SOP^L$ ), and the probability of strictly positive secrecy capacity (SPSC) are derived by using the classic Wyner's wiretap model. Two different scenarios for the fading parameters, i.e.,  $\mu$  and  $m$  which represents the shadowing impact have been studied. These parameters are chosen first as arbitrary numbers, thus the performance metrics are expressed in single infinite series with multivariate Meijer  $G$ -function. In the second scenario, both the aforementioned fading parameters are assumed to be integer numbers in order to obtain the derived results in simple exact closed-form analytic mathematically tractable expressions. The numerical results of this analysis are verified via Monte Carlo simulations.

## Index Terms

Average secrecy capacity, secure outage probability, probability of strictly positive secrecy capacity,  $\kappa - \mu$  shadowed fading.

## I. INTRODUCTION

Wyner has developed the information-theoretic notion of perfect secrecy that was introduced by Shannon via proposing the wiretap channel. The notion of this channel includes a legitimate user communicates with the intended receiver which are named Alice and Bob, respectively, in the presence of an eavesdropper [1]. Accordingly, the performance analysis of the physical layer security over fading channels has been given a special attention in the recent works. For example, the probability of strictly positive secrecy capacity (SPSC), the secure outage probability (SOP), and the average secrecy capacity (ASC) when the wireless channels undergo the additive white Gaussian noise (AWGN) and the Rayleigh fading channel are derived in [2] and [3]. The SPSC when both the main and wiretap channels undergo Rician fading

scenario is given in [4]. The SOP and SPSC over Rician/Nakagami- $m$  and Nakagami- $m$ /Rician fading scenarios are provided in [5]. The SPSC and the ASC of the Weibull fading channel are introduced in [6] and [7], respectively. The closed-form expression of SPSC when both the Bob and the eavesdropper experience log-normal fading is presented in [8].

Recently, many efforts have been devoted to study the secrecy performance of the physical layer over different generalized fading channels which give results closer to the practical measurement than the traditional distributions. For instance, the closed-form expressions for the SPSC and the lower bound of SOP ( $SOP^L$ ) over generalised Gamma fading model are derived by using the classic Wyner's wiretap model [9]. The analysis in [10] is investigated by analysing the SPSC and  $SOP^L$  over  $\kappa - \mu$  fading that is used to model the line-of-sight (LoS) communication scenario where the parameters  $\kappa$  and  $\mu$  denote the ratio between the powers of the dominant and the scattered waves components and the number of multipath clusters, respectively. In [11] and [12], the SPSC and the ASC are, respectively, utilised to analyse the secrecy performance over  $\alpha - \mu$  fading which is proposed to represent the non-homogeneous environment of wireless channel where  $\alpha$  indicates the non-linearity index. The scenarios of mean/wiretap channels undergo  $\alpha - \mu/\kappa - \mu$  and  $\kappa - \mu/\alpha - \mu$  fading conditions are given in [13] to study the secrecy capacity of physical layer via deriving the expression of the SPSC, the SOP, and the  $SOP^L$ .

The wireless channel may subject to the shadowing effect which is part of fading that can not be ignored. Hence, several works have been dedicated to analyse the security of physical layer over composite multipath/shadowed fading channels. The generalised- $K$  ( $GK$ ) fading model which is composite of Nakagami- $m$ /log-normal is employed to represent the main/wiretap channels of the classic Wyner's framework in [14] and [15]. In the former, the ASC, the SOP, and the SPSC are expressed in terms of the extended generalized bivariate Meijer  $G$ -function (EGBMGF) whereas a mixture Gamma distribution is used in the latter to approximate with high accuracy the same performance metrics. The analysis in [16] is based on using the  $\kappa - \mu$  shadowed fading channels to derive the SPSC, and the  $SOP^L$  of physical layer. However, the provided expressions are approximated and included the EGBMGF as well as two infinite series that are not easily and steadily convergence. Therefore, the authors have used the Gamma distribution to approximate the expressions of the aforementioned performance metrics in simple closed-form formats.

Unlike [16], this work analyses the secrecy performance of the physical layer over  $\kappa - \mu$  shadowed fading channel via different formats of the ASC, the SOP, the  $SOP^L$ , and the SPSC. The aforementioned

metrics are expressed first in single infinite series and the EGBMGF which would make the convergence acceleration is faster in comparison with [16]. In the second scenario, the parameter  $\mu$  and the shadowing severity index are supposed to be integer numbers. Consequently, the derived results are given in simple exact analytic mathematically tractable closed-form expressions. Furthermore, in [16], an approximation is utilised to obtain the closed-form expression of the SOP. It is remarkable that the ASC and the SOP in  $\kappa - \mu$  shadowed fading have not been provided in [16].

*Organization:* Section II describes the general and limited formats of the probability density function (PDF) and the cumulative distribution function of  $\kappa - \mu$  shadowed fading. The ASC, the SOP, the  $SOP^L$ , and the SPSC for general and integer values of  $\mu$  and shadowing parameters are derived in Sections III, IV, V, and VI, respectively. Section VII performs the Monte Carlo simulation and numerical results. Finally, conclusions are presented in Section VIII.

## II. THE PDF AND CDF OF $\kappa - \mu$ SHADOWED FADING

The PDF of the instantaneous SNR  $\gamma_i$ ,  $f_{\gamma_i}(\gamma_i)$ , for the destination (Bob),  $D$ , and the eavesdropper,  $E$ , channels in  $\kappa - \mu$  shadowed fading model is given by [17, eq. (4)]

$$f_{\gamma_i}(\gamma_i) = \Theta_i \gamma_i^{\mu_i - 1} e^{-\mathcal{A}_i \gamma_i} {}_1F_1(m_i; \mu_i; \mathcal{B}_i \gamma_i). \quad (1)$$

where  $i \in \{D, E\}$ ,  $\Theta_i = \frac{\mu_i m_i^{m_i} (1 + \kappa_i)^{\mu_i}}{\Gamma(\mu_i) \bar{\gamma}_i^{\mu_i} (\mu_i \kappa_i + m_i)^{m_i}}$ ,  $\mathcal{A}_i = \frac{\mu_i (1 + \kappa_i)}{\bar{\gamma}_i}$ ,  $\mathcal{B}_i = \frac{\mu_i^2 \kappa_i (1 + \kappa_i)}{(\mu_i \kappa_i + m_i) \bar{\gamma}_i}$ ,  $\bar{\gamma}_i$  is the average SNR,  $m_i$  is the shadowing severity index, and  ${}_1F_1(\cdot; \cdot; \cdot)$  is the confluent hypergeometric function defined in [18, eq. (9.14.1)].

The CDF of the  $\kappa - \mu$  shadowed fading channel is expressed as [17, eq. (6)]

$$F_{\gamma_i}(\gamma_i) = \frac{\Theta_i}{\mu_i} \gamma_i^{\mu_i} \Phi_2(\mu_i - m_i, m_i; \mu_i - 1; -\mathcal{A}_i \gamma_i, \mathcal{C}_i \gamma_i). \quad (2)$$

where  $\mathcal{C}_i = \frac{m_i}{\mu_i \kappa_i + m_i} \mathcal{A}_i$ ,  $\Phi_2(\cdot, \cdot; \cdot, \cdot; \cdot, \cdot)$  is the bivariate confluent hypergeometric function [18, eq. (9.261.2)].

When both  $\mu$  and  $m$  are integer numbers, i.e.,  $\mu$  and  $m \in \mathbb{Z}^+$ , the PDF and the CDF are, respectively, given by [19, eqs. (12) and eq. (13)]

$$f_{\gamma_i}(\gamma_i) = \sum_{j_i=0}^{M_i} \Lambda_{j_i} \frac{\gamma_i^{\psi_{j_i} - 1}}{\Omega_{j_i}^{\psi_{j_i}} (\psi_{j_i} - 1)!} e^{-\frac{\gamma_i}{\Omega_{j_i}}}. \quad (3)$$

and

$$F_{\gamma_i}(\gamma_i) = 1 - \sum_{j_i=0}^{M_i} \Lambda_{j_i} e^{-\frac{\gamma_i}{\Omega_{j_i}}} \sum_{r_i=0}^{\psi_{j_i} - 1} \frac{1}{r_i!} \left( \frac{\gamma_i}{\Omega_{j_i}} \right)^{r_i}. \quad (4)$$

TABLE I  
PARAMETER VALUES FOR THE PDF AND THE CDF OF THE  $\kappa - \mu$  SHADOWED FADING WITH INTEGER  $\mu$  AND  $m$  [19].

Case	Parameters
$\mu_i > m_i$	$M_i = \mu_i$ $\Lambda_{j_i} = \begin{cases} 0, & j_i = 0 \\ (-1)^{m_i} \binom{m_i+j_i-2}{j_i-1} \left[\frac{C_i}{A_i}\right]^{m_i} \left[\frac{B_i}{A_i}\right]^{-m_i-j_i+1}, & 0 < j_i \leq \mu_i - m_i \\ (-1)^{j_i-\mu_i+m_i-1} \binom{j_i-2}{j_i-\mu_i+m_i-1} \left[\frac{C_i}{A_i}\right]^{j_i-\mu_i+m_i-1} \left[\frac{B_i}{A_i}\right]^{-j_i+1}, & \mu_i - m_i < j_i \leq \mu_i \end{cases}$ $\psi_{j_i} = \begin{cases} \mu_i - m_i - j_i + 1, & 0 \leq j_i \leq \mu_i - m_i \\ \mu_i - j_i + 1, & \mu_i - m_i < j_i \leq \mu_i \end{cases}$ $\Omega_{j_i} = \begin{cases} \frac{1}{A_i}, & 0 \leq j_i \leq \mu_i - m_i \\ \frac{1}{C_i}, & \mu_i - m_i < j_i \leq \mu_i \end{cases}$
$\mu_i \leq m_i$	$M_i = m_i - \mu_i$ $\Lambda_{j_i} = \binom{m_i-\mu_i}{j_i} \left[\frac{C_i}{A_i}\right]^{j_i} \left[\frac{B_i}{A_i}\right]^{m_i-\mu_i-j_i}$ $\psi_{j_i} = m_i - j_i$ $\Omega_{j_i} = \frac{1}{C_i}$

where  $M_i$ ,  $\Lambda_{j_i}$ ,  $\psi_{j_i}$ , and  $\Omega_{j_i}$  are provided in Table I.

### III. AVERAGE SECRECY CAPACITY

The ASC can be calculated by  $\bar{C}_s = I_1 + I_2 - I_3$  [15, eq. (6)] where  $I_1$ ,  $I_2$ , and  $I_3$  are expressed as

$$I_1 = \int_0^\infty \ln(1 + \gamma_D) f_D(\gamma_D) F_E(\gamma_D) d\gamma_D. \quad (5)$$

$$I_2 = \int_0^\infty \ln(1 + \gamma_E) f_E(\gamma_E) F_D(\gamma_E) d\gamma_E. \quad (6)$$

$$I_3 = \int_0^\infty \ln(1 + \gamma_E) f_E(\gamma_E) d\gamma_E. \quad (7)$$

For arbitrary values of  $\mu$  and  $m$ ,  $I_1$ ,  $I_2$ , and  $I_3$  are, respectively, given by (8), (9), and (10)

$$I_1 = \Theta_D \Theta_E \frac{\Gamma(\mu_D) \Gamma(\mu_E)}{\Gamma(\mu_D - m_D) \Gamma(\mu_E - m_E) \Gamma(m_E)} \sum_{j=0}^{\infty} \frac{\mathcal{C}_E^j}{j!} \\ \times G_{1,0:2,2:1,2:2,2}^{0,1:1,2:1,1:1,2} \left( \begin{matrix} 1-j-\mu_D-\mu_E & 1,1 & 1-\mu_D+m_D & 1-\mu_E+m_E, 1-m_E \\ - & 1,0 & 0, 1-\mu_D & 0, -\mu_E-j \end{matrix} \middle| \frac{1}{\mathcal{A}_D - \mathcal{B}_D}, \frac{\mathcal{B}_D}{\mathcal{A}_D - \mathcal{B}_D}, \frac{\mathcal{A}_E}{\mathcal{A}_D - \mathcal{B}_D} \right). \quad (8)$$

$$I_2 = \Theta_E \Theta_D \frac{\Gamma(\mu_E) \Gamma(\mu_D)}{\Gamma(\mu_E - m_E) \Gamma(\mu_D - m_D) \Gamma(m_D)} \sum_{j=0}^{\infty} \frac{\mathcal{C}_D^j}{j!} \\ \times G_{1,0:2,2:1,2:2,2}^{0,1:1,2:1,1:1,2} \left( \begin{matrix} 1-j-\mu_E-\mu_D & 1,1 & 1-\mu_E+m_E & 1-\mu_D+m_D, 1-m_D \\ - & 1,0 & 0, 1-\mu_E & 0, -\mu_D-j \end{matrix} \middle| \frac{1}{\mathcal{A}_E - \mathcal{B}_E}, \frac{\mathcal{B}_E}{\mathcal{A}_E - \mathcal{B}_E}, \frac{\mathcal{A}_D}{\mathcal{A}_E - \mathcal{B}_E} \right). \quad (9)$$

$$I_3 = \Theta_E \frac{\Gamma(\mu_E)}{\Gamma(\mu_E - m_E)} G_{1,0:2,2:1,2}^{0,1:1,2:1,1} \left( \begin{matrix} 1-\mu_E & 1,1 & 1-\mu_E+m_E \\ - & 1,0 & 0, 1-\mu_E \end{matrix} \middle| \frac{1}{\mathcal{A}_E - \mathcal{B}_E}, \frac{\mathcal{B}_E}{\mathcal{A}_E - \mathcal{B}_E} \right). \quad (10)$$

where  $\Gamma(a) = \int_0^{\infty} x^{a-1} e^{-x} dx$  and  $G(\cdot)$  are the incomplete Gamma function and the EGBMGF as in [20, Table I], respectively. It can be noticed that the EGBMGF is not yet implemented in MATLAB and MATHEMATICA software packages. Therefore, a MATHEMATICA code that is available in [20] has been used in this work.

*Proof:* See Appendix A. ■

When both  $\mu$  and  $m$  are integer numbers, (5), (6), and (7) can be yielded in simple exact closed-form as follows

$$I_1 = \sum_{j_D=0}^{M_D} \Lambda_{j_D} \left[ e^{\mathcal{C}_{j_D}} \sum_{k=1}^{\psi_{j_D}} \frac{\Gamma(k - \psi_{j_D}, \mathcal{C}_{j_D})}{\Omega_{j_D}^{\psi_{j_D} - k}} \right. \\ \left. - \sum_{j_E=0}^{M_E} \Lambda_{j_E} e^{\mathcal{C}_{j_D} + \mathcal{C}_{j_E}} \sum_{r_E=0}^{\psi_{j_E} - 1} \frac{(\psi_{j_D})_{r_E}}{r_E!} \sum_{l=1}^{\psi_{j_D} + r_E} \frac{\Gamma(l - \psi_{j_D} - r_E, \mathcal{C}_{j_D} + \mathcal{C}_{j_E})}{\Omega_{j_D}^{\psi_{j_D} - l} \Omega_{j_E}^{r_E - l} (\Omega_{j_D}^{\psi_{j_D}} + \Omega_{j_E}^{\psi_{j_E}})^l} \right]. \quad (11)$$

$$I_2 = \sum_{j_E=0}^{M_E} \Lambda_{j_E} \left[ e^{\mathcal{C}_{j_E}} \sum_{k=1}^{\psi_{j_E}} \frac{\Gamma(k - \psi_{j_E}, \mathcal{C}_{j_E})}{\Omega_{j_E}^{\psi_{j_E} - k}} - \sum_{j_D=0}^{M_D} \Lambda_{j_D} e^{\mathcal{C}_{j_E} + \mathcal{C}_{j_D}} \sum_{r_D=0}^{\psi_{j_D} - 1} \frac{(\psi_{j_E})_{r_D}}{r_D!} \sum_{l=1}^{\psi_{j_E} + r_D} \frac{\Gamma(l - \psi_{j_E} - r_D, \mathcal{C}_{j_E} + \mathcal{C}_{j_D})}{\Omega_{j_E}^{\psi_{j_E} - l} \Omega_{j_D}^{r_D - l} (\Omega^{\psi_{j_E}} + \Omega^{\psi_{j_D}})^l} \right]. \quad (12)$$

$$I_3 = \sum_{j_E=0}^{M_E} \Lambda_{j_E} e^{\mathcal{C}_{j_E}} \sum_{k=1}^{\psi_{j_E}} \frac{\Gamma(k - \psi_{j_E}, \mathcal{C}_{j_E})}{\Omega_{j_E}^{\psi_{j_E} - k}} \quad (13)$$

where  $\Gamma(a, b) = \int_b^\infty x^{a-1} e^{-x} dx$  is the upper incomplete Gamma function [18, eq. (3.351.2)].

*Proof:* See Appendix B. ■

It can be observed that the ASC has not been presented in [16]. Consequently, to the authors' best knowledge, the expressions in (8)-(13) are novel.

#### IV. SECURE OUTAGE PROBABILITY

The SOP can be computed by [9, eq. (4)]

$$\text{SOP} = \int_0^\infty F_D(\theta\gamma_E + \theta - 1) f_E(\gamma_E) d\gamma_E \quad (14)$$

where  $\theta = \exp(R_s) \geq 1$  with  $R_s \geq 0$  denotes the target secrecy threshold.

When  $\mu$  and  $m \in \mathbb{N}^+$ , the SOP is expressed as

$$\begin{aligned} \text{SOP} &= \frac{\Theta_D \Theta_E}{\mu_D} \frac{\Gamma(\mu_E)}{\Gamma(\mu_E - m_E)} \sum_{i=0}^{\infty} \sum_{j=0}^{\infty} \frac{(\theta - 1)^{\mu_D + i + j} (-\mathcal{A}_D)^i \mathcal{C}_D^j}{\Gamma(-\mu_D - i - j) (\mathcal{A}_E - \mathcal{B}_E)^{\mu_E}} \\ &\times G_{1,0:1,1:1,2}^{0,1:1,1:1,1} \left( \begin{matrix} 1 - \mu_E & \mu_D + i + j + 1 \\ - & 0 \end{matrix} \middle| \begin{matrix} 1 - \mu_E + m_E \\ 0, 1 - \mu_E \end{matrix} \middle| \frac{\theta}{\theta - 1}, \frac{\mathcal{B}_E}{\mathcal{A}_E - \mathcal{B}_E} \right). \end{aligned} \quad (15)$$

For integer values of the fading parameters, the SOP is given in simple exact mathematically tractable closed-form expression as

$$\begin{aligned} \text{SOP} &= 1 - \sum_{j_D=0}^{M_D} \Lambda_{j_D} e^{-\frac{\theta-1}{\Omega_{j_D}}} \sum_{r_D=0}^{\psi_{j_D} - 1} \frac{1}{\Omega_{j_D}^{r_D} r_D!} \sum_{j_E=0}^{M_E} \frac{\Lambda_{j_E}}{\Omega_{j_E}^{\psi_{j_E}} (\psi_{j_E} - 1)!} \\ &\times \sum_{k=0}^{r_D} \binom{r_D}{k} \frac{\theta^k}{(\theta - 1)^{k - r_D} \left( \frac{\theta}{\Omega_{j_D}} + \frac{1}{\Omega_{j_E}} \right)^{k + \psi_{j_E}}} \Gamma(k + \psi_{j_E}) \end{aligned} \quad (16)$$

where  $\binom{b}{a} \triangleq \frac{b!}{(b-a)!}$  is the binomial coefficient.

*Proof:* See Appendix C. ■

One can see that the SOP in (15) and (16) are new because they have not been derived in the previous works such as [16].

## V. LOWER BOUND OF SOP

According to [6], the  $\text{SOP}^L$  can be obtained from (14) by inserting  $\gamma_E \rightarrow \infty$ . Hence, the  $\text{SOP}^L$  can be calculated by

$$\begin{aligned} \text{SOP}^L &= \int_0^\infty F_D(\theta\gamma_E) f_E(\gamma_E) d\gamma_E \\ &\leq \text{SOP} \end{aligned} \quad (17)$$

The  $\text{SOP}^L$  for arbitrary numbers of  $\mu$  and  $m$ , the  $\text{SOP}^L$  can be expressed in terms of a single infinite series as follows

$$\begin{aligned} \text{SOP}^L &= \Theta_D \Theta_E \theta^{\mu_D} \frac{\Gamma(\mu_D) \Gamma(\mu_E)}{\Gamma(\mu_E - m_E) \Gamma(\mu_D - m_D) \Gamma(m_D)} \sum_{j=0}^{\infty} \frac{(\theta \mathcal{C}_D)^j}{j!} (\mathcal{A}_E - \mathcal{B}_E)^{-(\mu_E + \mu_D + j)} \\ &\times G_{1,0:2,2:1,2}^{0,1:1,2:1,1} \left( \begin{matrix} 1 - \mu_E - \mu_D - j \\ - \end{matrix} \middle| \begin{matrix} 1 - \mu_D + m_D, 1 - m_D \\ 0, -\mu_D - j \end{matrix} \middle| \begin{matrix} 1 - \mu_E + m_E \\ 0, 1 - \mu_E \end{matrix} \middle| \frac{\theta \mathcal{A}_D}{\mathcal{A}_E - \mathcal{B}_E}, \frac{\mathcal{B}_E}{\mathcal{A}_E - \mathcal{B}_E} \right). \end{aligned} \quad (18)$$

When the values of both  $\mu$  and  $m$  are integer, the  $\text{SOP}^L$  can be obtained in simple exact closed-form expression as

$$\text{SOP}^L = 1 - \sum_{j_E=0}^{M_E} \frac{\Lambda_{j_E}}{\Omega_{j_E}^{\psi_{j_E}} (\psi_{j_E} - 1)!} \sum_{j_D=0}^{M_D} \Lambda_{j_D} \sum_{r_D=0}^{\psi_{j_D}-1} \frac{\theta^{r_D}}{\Omega_{j_D}^{\psi_{j_D}} r_D!} \frac{\Gamma(\psi_{j_E} + r_D)}{\left(\frac{\theta}{\Omega_{j_D}} + \frac{1}{\Omega_{j_E}}\right)^{\psi_{j_E} + r_D}} \quad (19)$$

*Proof:* See Appendix D. ■

## VI. PROBABILITY OF STRICTLY POSITIVE SECRECY CAPACITY

The SPSC can be obtained by [9, eq. (12)]

$$\text{SPSC} = 1 - \text{SOP} \quad \text{for } \theta = 1 \quad (20)$$

Accordingly, the SPSC for arbitrary and integer values of fading parameters can be deduced from (15) and (16), respectively, after using  $\theta = 1$  and plugging the results in (20).

## VII. PHYSICAL LAYER SECURITY OVER SPECIAL CASES OF $\kappa - \mu$ SHADOWED FADING MODEL

The secrecy performance over several main/wiretap fading scenarios can be deduced from the results of the  $\kappa - \mu$  shadowed fading by setting the fading parameters for a certain value. For example, when  $\kappa \rightarrow 0$ ,  $\mu = 1$ , and  $m \rightarrow \infty$ ,  $\kappa \rightarrow 0$ ,  $\mu = m$ ,  $m \rightarrow \infty$ , the wireless channels undergo Rayleigh and Nakagami-m fading conditions, respectively. The Rician and Rician shadowed fading models can be obtained by plugging  $\kappa = K$ ,  $\mu = 1$ , and  $m \rightarrow \infty$ ,  $\kappa = K$ ,  $\mu = 1$ ,  $m = m$ , respectively. The performance metrics of [10], i.e., the SPSC and the ASC over  $\kappa - \mu$  fading can be yielded by substituting  $\kappa = K$ ,  $\mu = \mu$ ,  $m \rightarrow \infty$  in the derived expressions.

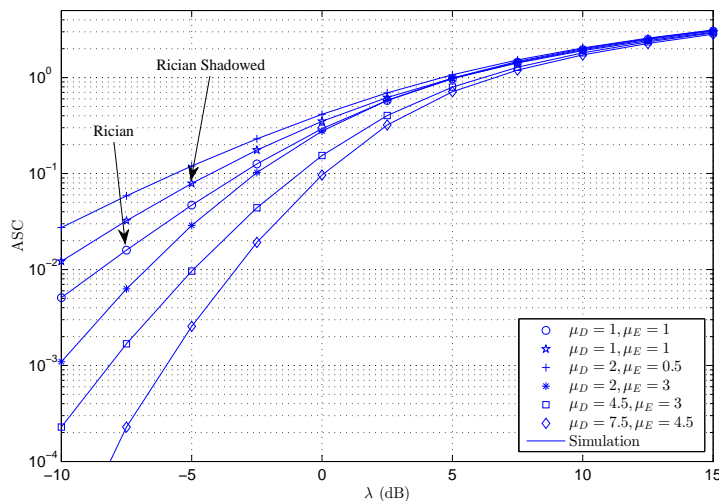


Fig. 1. ASC versus  $\lambda$  for different values of  $\mu_D$ ,  $\mu_E$ ,  $\kappa_D = \kappa_E = 3$ , and  $m_D = m_E = 2$ .

## VIII. NUMERICAL AND SIMULATION RESULTS

In this section, the numerical results of this work are verified via Monte Carlo simulations with  $10^7$  iterations. The parameters of main and wiretap channels are assumed to be independent and non-identically distributed random variables. In all figures, the markers represents the numerical results, whereas the solid lines explain the simulations. Furthermore, all the secrecy performance metrics are plotted versus the ratio  $\lambda = \bar{\gamma}_D/\bar{\gamma}_E$  and various values of  $\mu$  and  $m$ .

Figs. 1 and 2 illustrate the ASC for different values of  $\mu_i$  and  $m_i$  ( $i \in \{D, E\}$ ), respectively, with  $\kappa_D = \kappa_E = 3$ . From both figures, one can see that the value of the ASC reduces when  $\mu_i$  or/and  $m_i$



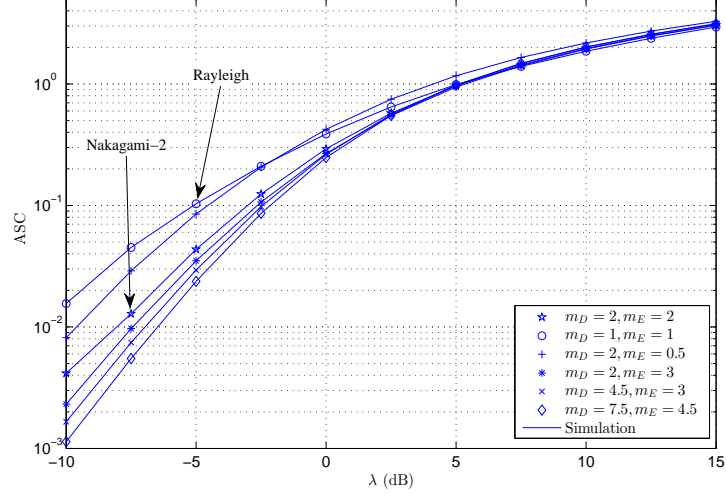


Fig. 2. ASC versus  $\lambda$  for different values of  $m_D$ ,  $m_E$ ,  $\kappa_D = \kappa_E = 3$ , and  $\mu_D = \mu_E = 2$ .

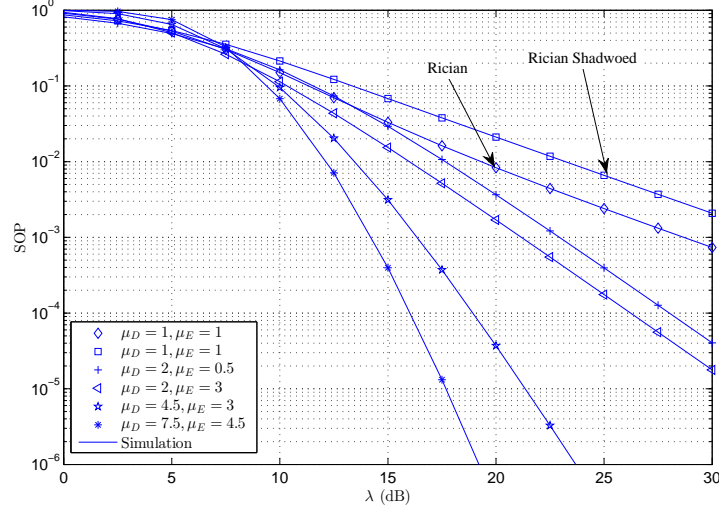


Fig. 3. SOP versus  $\lambda$  for different values of  $\mu_D$ ,  $\mu_E$ ,  $\kappa_D = \kappa_E = 3$ ,  $m_D = m_E = 2$ , and  $R_s = 1$ .

( $i \in \{D, E\}$ ) increase. This is because the high value of  $\mu$  and  $m$  refers to the large number of multipath clusters and less shadowing impact at the receiver (Bob or Eve). For instance, in Fig. 1, at  $\mu_D = 2$  and  $\lambda = -5$  dB (fixed), the ASC for  $\mu_E = 0.5$  is nearly 76% high than  $\mu_E = 3$ . In the same context, when  $\mu_E = 3$  and  $\mu_D$  changes from 2 to 4.5, the ASC is decreased by roughly 66.5%. On the other side, in Fig. 2, when  $m_D = 2$  at  $\lambda = -5$  dB (fixed), the values of the ASC for  $m_E = 0.5$  and  $m_E = 3$  are approximately 0.085 and 0.035, respectively. In addition, the same figure shows the ASC for  $m_D = 4.5$  is less than  $m_D = 2$  by roughly 16% at constant  $\lambda = -5$  dB and  $m_E = 3$ .

Figs. 3 and 4 demonstrate the SOP for for different values of  $\mu_i$  and  $m_i$  ( $i \in \{D, E\}$ ), respectively, with  $\kappa_D = \kappa_E = 3$ , and  $R_s = 1$ . It can be noticed from these figures that the SOP decreases with the

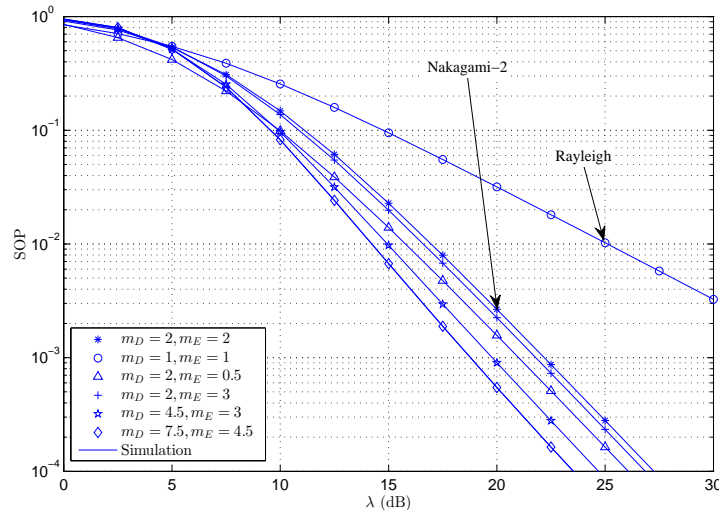


Fig. 4. SOP versus  $\lambda$  for different values of  $m_D, m_E, \kappa_D = \kappa_E = 3, \mu_D = \mu_E = 2$ , and  $R_s = 1$ .

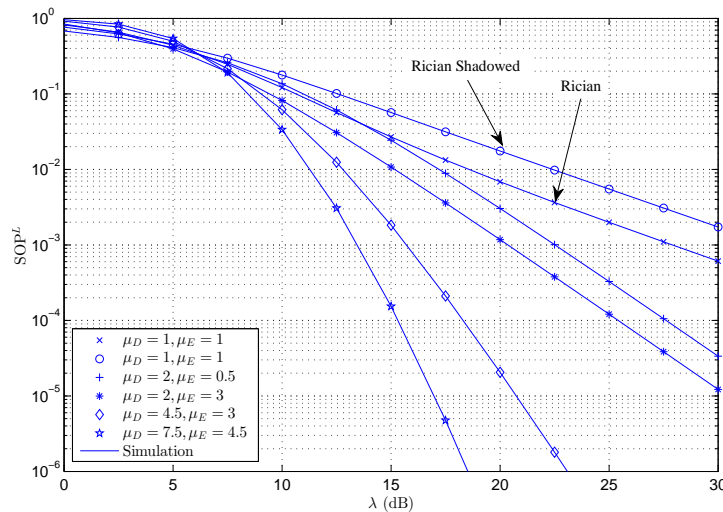


Fig. 5.  $SOP^L$  versus  $\lambda$  for different values of  $\mu_D, \mu_E, \kappa_D = \kappa_E = 3, m_D = m_E = 2$ , and  $R_s = 1$ .

rising of  $\mu_i$  or/and  $m_i$  ( $i \in \{D, E\}$ ) and for the same reasons that have been mentioned previously. For example, in Fig. 3, at  $\lambda = 15$  dB (fixed), the value of the SOP for the  $(\mu_D, \mu_E) = (7.5, 4.5)$  is less by nearly 87% and 98% than  $(\mu_D, \mu_E) = (4.5, 3)$  and  $(\mu_D, \mu_E) = (2, 0.5)$ , respectively. The provided results in Figs. 3 and 4 are, respectively, affirmed by Figs. 5 and 6 that explain the  $SOP^L$  for the same fading and simulation parameters. This confirmation comes from all the results in the latter figures are less than or equal to their corresponding scenarios in Figs. 3 and 4.

Figs. 7 and 8 explain the SPSC for different values of  $\mu_i$  and  $m_i$  ( $i \in \{D, E\}$ ), respectively, with  $\kappa_D = \kappa_E = 3$ . As expected, the SPSC decreases with the increasing in the fading parameters ( $\mu$  and  $m$ ) of the main or/and the wiretap channels.

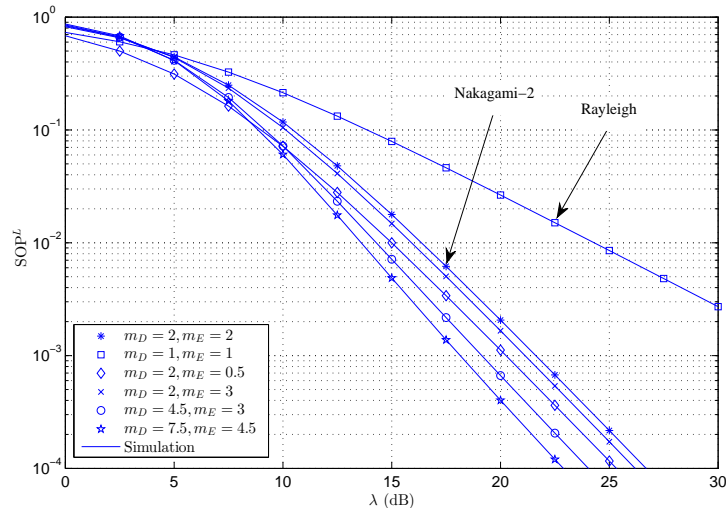


Fig. 6.  $SOP^L$  versus  $\lambda$  for different values of  $m_D$ ,  $m_E$ ,  $\kappa_D = \kappa_E = 3$ ,  $\mu_D = \mu_E = 2$ , and  $R_s = 1$

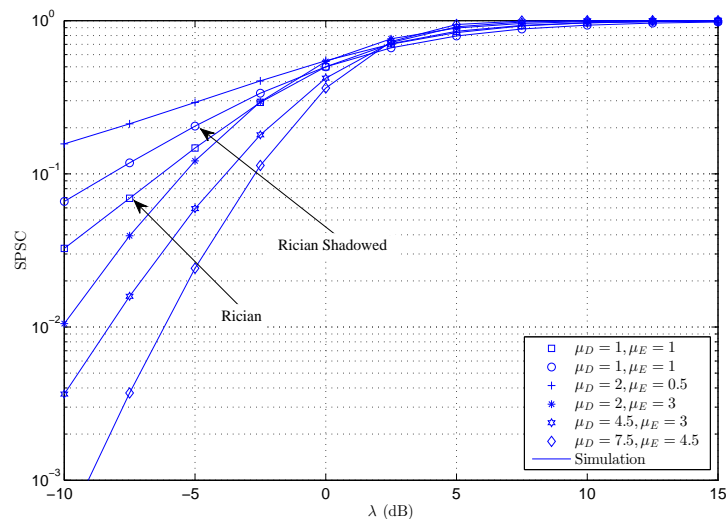


Fig. 7. SPSC versus  $\lambda$  for different values of  $\mu_D$ ,  $\mu_E$ ,  $\kappa_D = \kappa_E = 3$ , and  $m_D = m_E = 2$ .

From all figures, it is clear that the performance improves when the ratio  $\lambda$  increases. This refers to the high  $\bar{\gamma}_D$  in comparison with the  $\bar{\gamma}_E$  which would lead to make the Alice-Bob channel better than the Alice-Eve channel. Moreover, some the performance metrics of physical layer security over special cases of  $\kappa - \mu$  shadowed, namely, Rayleigh, Nakagami- $m$ , Rician, and Rician shadowed fading channels, have been also investigated. More importantly, the numerical results and Monte Carlo simulations are in perfect match for any provided scenario.

## IX. CONCLUSIONS

This paper was dedicated to study the secrecy behaviour of the physical layer over  $\kappa - \mu$  shadowed fading channels. Different performance metrics, such as the ASC, the SOP, the  $SOP^L$ , and the SPSC, were

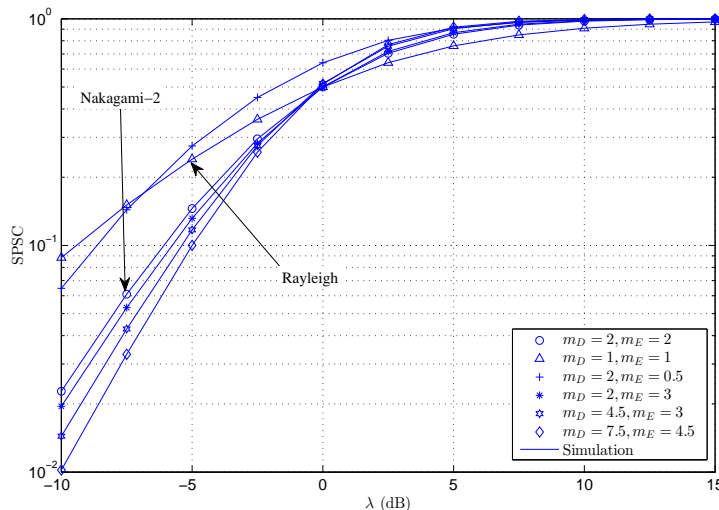


Fig. 8. SPSC versus  $\lambda$  for different values of  $m_D$ ,  $m_E$ ,  $\kappa_D = \kappa_E = 3$ , and  $\mu_D = \mu_E = 2$ .

derived by assuming two scenarios for the values of the fading parameters, namely, arbitrary and integer numbers. In the first scenario, the derived results were expressed in terms of EGBMGF and a single infinite series. On the other side, the second scenarios provided simple exact mathematically tractable closed-form expressions. From the given results, a reduction in the values of the ASC, the SOP, the  $SOP^L$ , and the SPSC can be observed when the values of  $\mu$  or/and  $m$  increase. Furthermore, the secrecy performances of some special cases of  $\kappa - \mu$  shadowed fading channels were also investigated. Accordingly, the results of this work can be employed to study the behaviour of the physical layer over a variety of fading channels with simple exact closed-form expressions and integer fading parameters.

## APPENDIX A

**Proof of (8):** Substituting (1) and (2) in (5), we have

$$I_1 = \frac{\Theta_D \Theta_E}{\mu_E} \int_0^\infty \ln(1 + \gamma_D) \gamma_D^{\mu_D + \mu_E - 1} e^{-\mathcal{A}_D \gamma_D} {}_1F_1(m_D; \mu_D; \mathcal{B}_D \gamma_D) \times \Phi_2(\mu_E - m_E, m_E; \mu_E - 1; -\mathcal{A}_E \gamma_D, \mathcal{C}_E \gamma_D) d\gamma_D. \quad (21)$$

With the help of [21, eq. (1.3.7)], [18, eq. (9.261.2)], [21, eq. (1.1.20)], and [18, eq. (9.14.1)], we have

$$\begin{aligned}
I_1 = & \Theta_D \Theta_E \frac{\Gamma(\mu_D) \Gamma(\mu_E)}{\Gamma(\mu_D - m_D) \Gamma(\mu_E - m_E) \Gamma(m_E)} \sum_{j=0}^{\infty} \frac{\mathcal{C}_E^j}{j!} \\
& \times \int_0^{\infty} \ln(1 + \gamma_D) \gamma_D^{\mu_D + \mu_E + j - 1} e^{-(\mathcal{A}_D - \mathcal{B}_D)\gamma_D} {}_1F_1(\mu_D - m_D; \mu_D; -\mathcal{B}_D \gamma_D) \\
& \times {}_2F_1(\mu_E - m_E, \mu_E; \mu_E + j + 1; -\mathcal{B}_D \gamma_D) d\gamma_D. \tag{22}
\end{aligned}$$

Using the identities [22, eq. (11)], [18, eq. (9.34.8)], and [18, eq. (9.34.7)] to express  $e^{-x}$  and  $\ln(1+x)$ ,  ${}_1F_1(x; y; -z)$ , and  ${}_2F_1(x_1, x_2; y; -z)$  in terms of Meijer  $G$ -function. Thus, (22) can be rewritten as

$$\begin{aligned}
I_1 = & \Theta_D \Theta_E \frac{\Gamma(\mu_D) \Gamma(\mu_E)}{\Gamma(\mu_D - m_D) \Gamma(\mu_E - m_E) \Gamma(m_E)} \sum_{j=0}^{\infty} \frac{\mathcal{C}_E^j}{j!} \\
& \times \int_0^{\infty} \gamma_D^{\mu_D + \mu_E + j - 1} G_{2,2}^{1,2} \left( \begin{matrix} 1, 1 \\ 1, 0 \end{matrix} \middle| \gamma_D \right) G_{0,1}^{1,0} \left( \begin{matrix} - \\ 0 \end{matrix} \middle| (\mathcal{A}_D - \mathcal{B}_D)\gamma_D \right) \\
& \times G_{1,2}^{1,1} \left( \begin{matrix} 1 - \mu_D + m_D \\ 0, 1 - \mu_D \end{matrix} \middle| \mathcal{B}_D \gamma_D \right) G_{2,2}^{1,2} \left( \begin{matrix} 1 - \mu_E - m_E, 1 - m_E \\ 0, -\mu_E - j \end{matrix} \middle| \mathcal{A}_E \gamma_D \right) d\gamma_D. \tag{23}
\end{aligned}$$

The integral in (23) can be computed by [23, eq. (9)] and that completes the proof of (8).

**Proof of (9):** It can be observed that (9) can be calculated by (8) after replacing the symbols  $D$  and  $E$  with  $E$  and  $D$ , respectively.

**Proof of (10):** Plugging (1) in (7), we have

$$I_3 = \Theta_E \int_0^{\infty} \ln(1 + \gamma_E) \gamma_E^{\mu_E - 1} e^{-\mathcal{A}_E \gamma_E} {}_1F_1(m_E; \mu_E; \mathcal{B}_E \gamma_E) d\gamma_E \tag{24}$$

Similar to (9), the identities [22, eq. (11)] and [18, eq. (9.34.8)] are utilised to obtain

$$\begin{aligned}
I_3 = & \Theta_E \frac{\Gamma(\mu_E)}{\Gamma(\mu_E - m_E)} \int_0^{\infty} \gamma_E^{\mu_E - 1} G_{2,2}^{1,2} \left( \begin{matrix} 1, 1 \\ 1, 0 \end{matrix} \middle| \gamma_E \right) \\
& \times G_{0,1}^{1,0} \left( \begin{matrix} - \\ 0 \end{matrix} \middle| (\mathcal{A}_E - \mathcal{B}_E)\gamma_E \right) G_{1,2}^{1,1} \left( \begin{matrix} 1 - \mu_E + m_E \\ 0, 1 - \mu_E \end{matrix} \middle| \mathcal{B}_E \gamma_E \right) d\gamma_E. \tag{25}
\end{aligned}$$

With the aid of [23, eq. (9)], (25) can be evaluated in exact closed-form expression as in (10).

## APPENDIX B

**Proof of (11):** After inserting (3) and (4) in (5), this yields

$$I_1 = \sum_{j_D=0}^{M_D} \frac{\Lambda_{j_D}}{\Omega_{j_D}^{\psi_{j_D}} (\psi_{j_D} - 1)!} \left[ \int_0^\infty \ln(1 + \gamma_D) \gamma_D^{\psi_{j_D} - 1} e^{-\frac{\gamma_D}{\Omega_{j_D}}} d\gamma_D \right. \\ \left. - \sum_{j_E=0}^{M_E} \Lambda_{j_E} \sum_{r_E=0}^{\psi_{j_E} - 1} \frac{1}{\Omega_{j_E}^{r_E} r_E!} \int_0^\infty \ln(1 + \gamma_D) \gamma_D^{\psi_{j_D} + r_E - 1} e^{-\left(\frac{1}{\Omega_{j_D}} + \frac{1}{\Omega_{j_E}}\right) \gamma_D} d\gamma_D \right]. \quad (26)$$

Employing [24, eq. (47)] to calculate the integrals of (26) in simple exact closed-form expressions as given in (11).

**Proof of (12):** Using  $D$  and  $E$  instead of  $E$  and  $D$ , respectively, in (11), the result is  $I_2$  that is given in (12).

**Proof of (13):** Plugging (3) in (7), this yields

$$I_3 = \sum_{j_E=0}^{M_E} \frac{\Lambda_{j_E}}{\Omega_{j_E}^{\psi_{j_E}} (\psi_{j_E} - 1)!} \int_0^\infty \ln(1 + \gamma_E) \gamma_E^{\psi_{j_E} - 1} e^{-\frac{\gamma_E}{\Omega_{j_E}}} d\gamma_E. \quad (27)$$

Likewise, [24, eq. (47)] is utilised to express (27) in exact closed-form as in (13).

## APPENDIX C

**Proof of (15):** Inserting (1) and (2) in (14) and using [18, eq. (9.261.2)] and [21, eq. (1.3.7)], the result is

$$\text{SOP} = \frac{\Theta_D \Theta_E}{\mu_D} \sum_{i=0}^{\infty} \sum_{j=0}^{\infty} (-\mathcal{A}_D)^i \mathcal{C}_D^j \\ \times \int_0^\infty (\theta \gamma_E + \theta - 1)^{\mu_D + i + j} \gamma_E^{\mu_E - 1} e^{-(\mathcal{A}_E - \mathcal{B}_E) \gamma_E} {}_1F_1(\mu_E - m_E; \mu_E; -\mathcal{B}_E \gamma_E) d\gamma_E \quad (28)$$

After doing some mathematical manipulations and recalling the identities [22, eq. (10)], [18, eq. (9.34.8)], and [22, eq. (17)], to write  $(1 + x)^a$ ,  $e^{-x}$ , and  ${}_1F_1(x; y; -z)$ , respectively, using Meijer  $G$ -

function, (28) becomes

$$\begin{aligned}
\text{SOP} &= \frac{\Theta_D \Theta_E}{\mu_D} \frac{\Gamma(\mu_E)}{\Gamma(\mu_E - m_E)} \sum_{i=0}^{\infty} \sum_{j=0}^{\infty} \frac{(\theta - 1)^{\mu_D + i + j} (-\mathcal{A}_D)^i \mathcal{C}_D^j}{\Gamma(-\mu_D - i - j)} \\
&\times \int_0^{\infty} \gamma_E^{\mu_E - 1} G_{0,1}^{1,0} \left( - \middle| \begin{array}{c} (\mathcal{A}_E - \mathcal{B}_E) \gamma_E \end{array} \right) \\
&\times G_{1,1}^{1,1} \left( \begin{array}{c} \mu_D + i + j + 1 \\ 0 \end{array} \middle| \frac{\theta}{\theta - 1} \gamma_E \right) G_{1,2}^{1,1} \left( \begin{array}{c} 1 - \mu_E + m_E \\ 0, 1 - \mu_E \end{array} \middle| \mathcal{B}_E \gamma_E \right) d\gamma_E. \tag{29}
\end{aligned}$$

With the aid of [23, eq. (9)], the expression of the SOP in (29) can be deduced as in (15) which completes the proof.

**Proof of (16):** Substituting (3) and (4) in (14) and utilising  $\int_0^{\infty} f_{\gamma}(\gamma) d\gamma \triangleq 1$ , we have

$$\begin{aligned}
\text{SOP} &= 1 - \sum_{j_D=0}^{M_D} \Lambda_{j_D} e^{-\frac{\theta-1}{\Omega_{j_D}}} \sum_{r_D=0}^{\psi_{j_D}-1} \frac{1}{\Omega_{j_D}^{r_D} r_D!} \sum_{j_E}^{M_E} \frac{\Lambda_{j_E}}{\Omega_{j_E}^{\psi_{j_E}} (\psi_{j_E} - 1)!} \\
&\times \int_0^{\infty} \gamma_E^{\psi_{j_E}-1} (\theta \gamma_E + \theta - 1)^{r_D} e^{-\left(\frac{\theta}{\Omega_{j_D}} + \frac{1}{\Omega_{j_E}}\right) \gamma_E} d\gamma_E \tag{30}
\end{aligned}$$

Doing some mathematical manipulations with the aid  $(1+a)^b = \sum_{k=0}^b \binom{b}{k} a^k$  [18, eq. (1.111)] and employing [18, eq. (3.381.4)], the integral of (30) can be expressed in simple exact closed-form as in (16).

#### APPENDIX D

**Proof of (18):** Inserting (1) and (2) in (17) and following the same procedure for (28), this yields

$$\begin{aligned}
\text{SOP}^L &= \Theta_D \Theta_E \theta^{\mu_D} \frac{\Gamma(\mu_D) \Gamma(\mu_E)}{\Gamma(\mu_E - m_E) \Gamma(\mu_D - m_D) \Gamma(m_D)} \sum_{j=0}^{\infty} \frac{(\theta \mathcal{C}_D)^j}{j!} \\
&\times \int_0^{\infty} \gamma_E^{\mu_E + \mu_D + j - 1} G_{0,1}^{1,0} \left( - \middle| \begin{array}{c} (\mathcal{A}_E - \mathcal{B}_E) \gamma_E \end{array} \right) \\
&\times G_{2,2}^{1,2} \left( \begin{array}{c} 1 - \mu_D + m_D, 1 - m_D \\ 0, -\mu_D - j \end{array} \middle| \theta \mathcal{A}_D \gamma_E \right) G_{1,2}^{1,1} \left( \begin{array}{c} 1 - \mu_E + m_E \\ 0, 1 - \mu_E \end{array} \middle| \mathcal{B}_E \gamma_E \right) d\gamma_E. \tag{31}
\end{aligned}$$

Again, [23, eq. (9)] is employed to evaluate the integral of (31) as given in (18) which completes the proof.

**Proof of (19):** Plugging (3) and (4) in (17) and employing  $\int_0^\infty f_\gamma(\gamma)d\gamma \triangleq 1$ , we have

$$\text{SOP}^L = 1 - \sum_{j_E=0}^{M_E} \frac{\Lambda_{j_E}}{\Omega_{j_E}^{\psi_{j_E}} (\psi_{j_E} - 1)!} \sum_{j_D=0}^{M_D} \Lambda_{j_D} \sum_{r_D=0}^{\psi_{j_D}-1} \frac{\theta^{r_D}}{\Omega_{j_D}^{\psi_{j_D}} r_D!} \int_0^\infty \gamma_E^{\psi_{j_E}+r_D-1} e^{-\left(\frac{\theta}{\Omega_{j_D}} + \frac{1}{\Omega_{j_E}}\right)\gamma_E} d\gamma_E \quad (32)$$

With the aid of [18, eq. (3.381.4)], (32) can be calculated in simple exact closed-form expression as provided in (19).

## REFERENCES

- [1] A. D. Wyner, "The wire-tap channel," *Bell Syst. Tech. J.*, vol. 54, no. 8, pp. 1355-1387, Oct. 1975.
- [2] J. Barros, M. R. D. Rodrigues, "Secrecy capacity of wireless channels," in *Proc. IEEE Int. Symp. Inf. Theory (ISIT)*, Seattle, WA, July 2006, pp. 356-360.
- [3] M. Bloch, J. Barros, M. R. D. Rodrigues, and S. W. McLaughlin, "Wireless information-theoretic security," *IEEE Trans. Inf. Theory*, vol. 54, no. 6, pp. 2515-2534, June 2008.
- [4] X. Liu, "Probability of strictly positive secrecy capacity of the Rician-Rician fading channel," *IEEE Wireless Commun. Lett.*, vol. 2, no. 1, pp. 50-53, Feb. 2013.
- [5] S. Iwata, T. Ohtsuki, and P. Y. Kam, "Performance analysis of physical layer security over Rician/Nakagami-m fading channels," in *Proc. IEEE Veh. Technol. Conf. (VTC Spring)*, Sydney, NSW, June 2017, pp. 1-6.
- [6] X. Liu, "Probability of strictly positive secrecy capacity of the Weibull fading channel," in *Proc. IEEE Global Commun. Conf. (GLOBECOM)*, Atlanta, GA, June 2013, pp. 659-664.
- [7] X. Liu, "Average secrecy capacity of the Weibull fading channel," in *Proc. IEEE Annual Consumer Commun. Net. Conf. (CCNC)*, Las Vegas, NV, 2016, pp. 841-844.
- [8] X. Liu, "Secrecy capacity of wireless links subject to log-normal fading," in *Proc. IEEE Conf. Commun. Net. (CCN)*, China, Kun Ming, Jan. 2012, pp. 167-172.
- [9] H. Lei, C. Gao, Y. Guo, and G. Pan, "On physical layer security over generalized gamma fading channels," *IEEE Commun. Lett.*, vol. 19, no. 7, pp. 1257-1260, July 2015.
- [10] N. Bhargav, S. L. Cotton, and David E. Simmons, "Secrecy capacity analysis over  $\kappa - \mu$  fading channels: Theory and applications," *IEEE Trans. Commun.*, vol. 164, no. 7, pp. 3011-3024, July 2016.
- [11] L. Kong, H. Tran, and G. Kaddoum, "Performance analysis of physical layer security over  $\alpha - \mu$  fading channel," *Electron. Lett.*, vol. 52, no. 1, pp. 45-47, Jan. 2016.
- [12] H. Lei, H. Zhang, I. S. Ansari, G. Pan, B. Alomair, and M. S. Alouini, "Secrecy capacity analysis over  $\alpha - \mu$  fading channels," *IEEE Commun. Lett.*, vol. 21, no. 6, pp. 1445-1448, June 2017.
- [13] N. Bhargav, and S. L. Cotton, "Secrecy capacity analysis for  $\alpha - \mu/\kappa - \mu$  and  $\kappa - \mu/\alpha - \mu$  fading scenarios," in *Proc. IEEE Pers., Indoor, and Mob. Radio Commun. (PIMRC)*, Valencia, 2016, pp. 1-6.
- [14] H. Lei, H. Zhang, I. S. Ansari, C. Gao., Y. Guo, G. Pan, and K. A. Qaraqe, "Physical layer security over generalized- $K$  fading channels," *IET Commun.*, vol. 10, no. 16, pp. 2233-2237, July 2016.
- [15] H. Lei, H. Zhang, I. S. Ansari, C. Gao., Y. Guo, G. Pan, and K. A. Qaraqe, "Performance analysis of physical layer security over generalized- $K$  fading channels using a mixture gamma distribution," *IEEE Commun. Lett.*, vol. 20, no. 2, pp. 408-411, Feb. 2016.
- [16] J. Sun, X. Li, M. Huang, Y. Ding, J. Jin, and G. Pan "Performance analysis of physical layer security over  $\kappa - \mu$  shadowed fading channels," *IET Commun.*, vol., no., pp., Feb. 2018.



- [17] J. F. Paris, "Statistical characterization of  $\kappa - \mu$  shadowed fading," *IEEE Trans. Veh. Technol.*, vol. 63, no. 2, pp. 518-526, Feb. 2014.
- [18] I. S. Gradshteyn, and I. M. Ryzhik, *Table of Integrals, Series and Products*, 7th edition. Academic Press Inc., 2007.
- [19] F. J. Lopez-Martinez, J. F. Paris and J. M. Romero-Jerez, "The  $\kappa$ -  $\mu$  shadowed fading model with integer fading parameters," *IEEE Trans. Veh. Technol.*, vol. 66, no. 9, pp. 7653-7662, Sept. 2017.
- [20] I. S. Ansari, S. Al-Ahmadi, F. Yilmaz, M.-S. Alouini, and H. Yanikomeroglu, "A new formula for the BER of binary modulations with dual-branch selection over generalized- $K$  composite fading channels," *IEEE Trans. Commun.*, vol. 59, no. 10, pp. 2654-2658, Oct. 2011.
- [21] H. M. Srivastava, and H. L. Manocha, *A treatise on generating functions*, Wiley, New York, 1984.
- [22] V. S. Adamchik and O. I. Marichev, "The algorithm for calculating integrals of hypergeometric type functions and its realization in REDUCE system," in *Proc. IEEE ISSAC*, Tokyo, Japan, Aug. 1990, pp. 212-224.
- [23] C. García-Corrales, F. J. Cañete, and J. F. Paris, "Capacity of  $\kappa - \mu$  shadowed fading channels," *Int. J. of Antennas and Propagation*, vol. 2014, pp. 1-8, July 2014.
- [24] J. Jung, S.-R. Lee, H. Park, S. Lee, and I. Lee, "Capacity and error probability analysis of diversity reception schemes over generalized- $K$  fading channels using a mixture gamma distribution," *IEEE Trans. Wireless Commun.*, vol. 13, no. 9, pp. 4721-4730, Sept. 2014.